Homogeneously Dispersed Ceria Nanocatalyst Stabilized with Ordered Mesoporous Alumina

By *Quan Yuan, Hao-Hong Duan, Le-Le Li, Zhen-Xing Li, Wen-Tao Duan, Le-Sheng Zhang, Wei-Guo Song,* and *Chun-Hua Yan**

As one of the most important functional rare earth oxides, ceria (CeO_2) has been widely applied in catalysis, fuel cells, optical materials, gas sensors, and so forth. In particular, nanostructured ceria plays an active role in catalysis applications because of its reduced dimensions, increased relative surface area, highly active facets, large number of active sites, and changeable valence state.[1] In the past decade, the controlled synthesis of ceria nanocrystals has become one of the essential topics in rare earth materials science, since high selectivity and activity can be achieved by size and morphology design.[2] One of the well-known cases is the role of CeO_2 in CO oxidation. In this case, traditional bulk ceria materials had been reported to be inadequate for CO oxidation as a catalyst support.[3] However, as shown by Corma et al. the activity for CO oxidation increased by two orders of magnitude when the particle size of ceria decreased to the nanosize region.[4] Hydrothermal, solvothermal, and thermolysis approaches, all of which are based on solution-phase methods, are widely utilized for nanostructured ceria synthesis.[5] Recent examples showed that sub-10-nm ceria can be synthesized using capping agents. Using oleic acid as the stabilizing agent, Gao and coworkers obtained monodisperse ceria nanocubes with an average size of approximatley 4 nm.[2b] However, an obstruction for further application lies in that CeO_2 nanoparticles with a size smaller than 5 nm tend to aggregate during thermal treatments, forming secondary large particles, and thus, the active sites decrease rapidly owing to reduced surfaces. Therefore, up to now, the synthesis of thermally stable ceria nanoparticles with a uniform small size still remains as a challenge.

In the case of catalysis reaction, catalyst deactivations caused by sintering of catalysts at high temperature are very common, which may hinder their further industrial applications. Confinement effect can be a solution to address this tough problem. Materials with different nanostructures, especially those that have pores or hollows, are ideal candidates to provide confined microenvironments. With ordered channels of 2–50 nm, mesoporous structured materials are very suitable for this purpose. Current methodologies for the assembly of metal or metal oxide nanoparticles in mesoporous materials include, for example, conventional incipient wetness impregnation,[6] post-grafting,[7] and metal–organic chemical vapor deposition.[8] Somorjai et al. incorporated Pt nanocrystals into SBA-15 silica during hydrothermal synthesis.[9] The Pt particles were observed to be located within surfactant micelles during silica formation, which led to their dispersion throughout the silica structure. Bao and co-workers reported an in situ autoreduction route for the fabrication of monodisperse silver nanoparticles on silica-based materials.[7] Features of the narrow channels in hexagonal mesostructures (for example MCM-41, SBA-15) being utilized, one-dimensional nanomaterials such as nanorods or nanowires can be anticipated. Gold nanowires have been reported in the channels of mesoporous SBA-15 by hydrogen flow reduction,[10] electroless reduction,[11] and seed-mediated growth processes.[12] CeO_2 nanoparticles were also embedded into mesoporous SiO_2 during the mesostructure formation and then stabilized by this ordered mesostructure.[13] Although many efforts have been devoted to explore the confinement effect of mesoporous materials, almost all of these works are focused on silica-based mesoporous materials except for a few works on carbon-based cases. Despite its obvious virtues, the lack of acid/base sites as well as the chemical inactive inertness of the silica surface limits its use for the purpose of catalysis application.

As a promising candidate for a three-way catalyst, CeO_2–Al_2O_3 composites have attracted world-wide attention. The sol–gel process was employed to synthesize the ceria-doped alumina materials reported by Viveros et al.[14] In our previous study, the ordered mesoporous aluminas have proved to possess wide applications in catalysis with the benefits of their large surface areas, high thermal stability, large surface Lewis acid sites, and tunable pore size.[15] They are proposed to be good candidates for the fabrication and stabilization of nanometer-scaled ceria, since the channels can prevent the possible growth and reuniting of nanocrystals. Based on all the advantages mentioned above, herein, using the sol–gel method combined with an evaporation-induced self-assembly process, we explore a new strategy to synthesize uniform ceria nanocatalysts stabilized by ordered mesoporous alumina.

Using the sample with 8 mol% Ce (denoted as meso-8CeAl) as an example, evidence for the formation of mesostructures is provided by small-angle X-ray diffraction (XRD) patterns shown in Figure 1a. The sample calcined at 400 °C shows a very strong diffraction peak around 1.0° and one weak peak around 1.7°, which, associated with transmission electron microscopy (TEM) observation, can be attributed to *p6mm* hexagonal symmetry. The mesoscopic ordering is sustained well even after calcination at

[*] Prof. C. H. Yan, Dr. Q. Yuan, H. H. Duan, L. L. Li, Z. X. Li, W. T. Duan
Beijing National Laboratory for Molecular Sciences
State Key Laboratory of Rare Earth Materials Chemistry and Applications
Peking University, Beijing, 100871 (P. R. China)
E-mail: yan@pku.edu.cn
Prof. W. G. Song, Dr. L. S. Zhang
Institute of Chemistry
Chinese Academy of Sciences
Beijing, 100190 (P. R. China)

DOI: 10.1002/adma.200904223

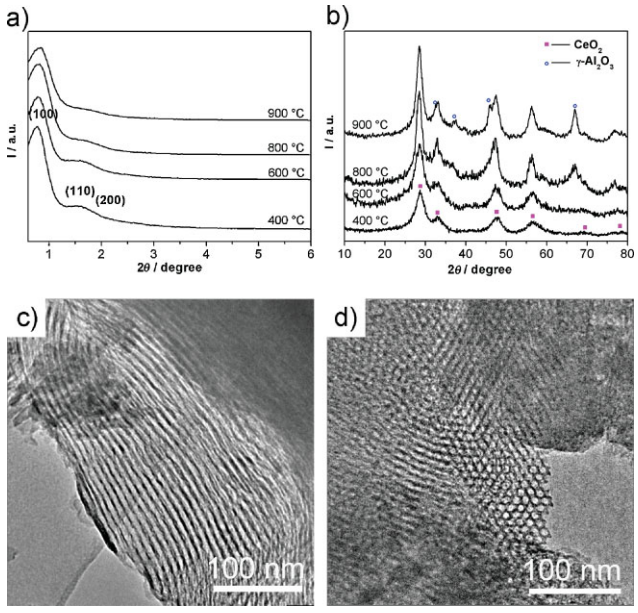

Figure 1. a) Small- and b) wide-angle XRD patterns of meso-8CeAl calcined at different temperatures. TEM images of meso-8CeAl calcined at 400 °C viewed along the c) [001] and d) [110] direction.

higher temperatures of 600, 800, and 900 °C, respectively. This indicates that the introduction of Ce in this one-step synthesis does not affect the formation of the mesoporous structure. However, it stabilizes the ordered mesoporous structure at high temperature. Figure 1b shows the corresponding wide-angle XRD patterns of meso-8CeAl calcined at different temperatures. Calcination at 400 °C gives a mesostructure with an amorphous wall, and thermal treatment at temperatures higher than 800 °C gives rise to a γ-Al_2O_3 phase (JCPDS Card No. 10-0425). The appearance of crystalline CeO_2 particles can be expected according to the diffraction peaks of (111), (200), (220), (311), (400), and (331), which correspond to a pure fluorite CeO_2 phase (JCPDS 34-0394, space group *Fm*3*m*). The CeO_2 particle size is estimated to be around 3–4 nm calculated from the Scherrer equation. TEM images confirm the typical 2D hexagonal mesostructures with a regular array of cylindrical mesopores viewed from the [110] direction (Fig. 1c) and an ordered hexagonal arrangement of pores along the [001] direction (Fig. 1d), which are in full agreement with the images of pure alumina in the aforementioned article.[15] Varying the content of cerium, a series of ordered mesostructures is obtained (Fig. S1 and Fig. S2).

High-angle annular dark-field scanning transmission electron microscopy (HAADF STEM) is known for its great sensitivity to the atomic number *Z*, which affords better contrasts than the dark and bright field operation modes. Figure 2a is the HAADF image of the meso-8CeAl sample. A very large number of bright spots can be detected on the mesoporous Al_2O_3 base, presumed to be CeO_2 nanoparticles which are highly dispersed on the external surface or in the mesopores. The HAADF image of meso-16CeAl shows a larger number of bright spots (Fig. 2b) and indicates that more CeO_2 nanoparticles form at a higher content of Ce, in accordance with the increased intensity of diffraction peaks in the wide-angle XRD data when the Ce/Al molar ratio increases. The average diameter of these particles is measured to be around 5 nm. The selected-area electron diffraction (SAED) pattern (Fig. 2c) shows a fluoride cubic structure, which is consistent with the phase of CeO_2. Lattice planes with a spacing of 0.31 nm are also present in the high-resolution TEM (HRTEM) image of an individual nanoparticle (Fig. 2d), which can be attributed to the (111) plane of CeO_2. Under the mode of HAADF STEM, energy-dispersive analysis of X-rays (EDX) is taken at different parts of the meso-8CeAl sample (Fig. S3). For the three positions selected as examples, the Ce/Al molar ratios calculated from the EDX data are 10.4, 9.0, and 10.7%, respectively (Table S1 in the Supporting Information), all of which are similar to that of the original molar ratio 8%. This indicates that the ceria particles are distributed homogeneously in the framework of the mesostructure, further confirming the observed results from HAADF STEM images.

To understand the chemical state of CeO_2 nanoparticles stabilized by mesoporous alumina, electron energy loss spectra (EELS) analysis in the M-edge region of cerium, which carries information of the initial-state 4*f* occupancy, is performed (Fig. 2e and 2f). Since electron-beam irradiation for extended periods risks damage with the valence change of Ce ions from Ce^{4+} to Ce^{3+}, we used a short EELS acquisition time of 2 s. For comparison, a pure CeO_2 thin film is also detected by EELS (Fig. 2e). The $M_{4,5}$ edges reflect transitions of 3d core electrons to unoccupied states of p- and f-like symmetry. EELS of the Ce L_3 edge spectrum of meso-8CeAl is close to that of Ce^{3+} (Fig. 2f). By normalizing Ce^{4+} and Ce^{3+} $M_{4,5}$ edges to the continuum above the edges, the Ce^{4+}/Ce^{3+} ratios can be determined. In this way, the integrated areas of the $M_{4,5}$ edges are quantifiably related and are able to reflect the ratio of f-holes of Ce^{4+} and Ce^{3+}. The spectrum of the CeO_2 thin film gives a M_4/M_5 intensity ratio of 0.93, which is the characteristic of Ce^{4+}; whereas the meso-8CeAl sample gives a ratio of 1.17. From the composition of these two ratios, the existence of Ce^{3+} in the obtained nanoparticles is confirmed and the fraction of Ce^{3+} is estimated to be 65%.[16] Furthermore, X-ray photoelectron spectroscopy (XPS), which is a surface chemical composition analysis technique, is used to determine the chemical valence of Ce on the material surface (Fig. S4b in the Supporting Information). Six Ce 3d binding-energy peaks are consistent with the previous report of Ce^{4+},[17] indicating that the main valence of cerium in the sample is +4. Meanwhile, two peaks due to a pair of doublets (noted as u_1, u_1'), which lie at 885.7 and 904.1 eV, are observed, which are characteristic of Ce^{3+} 3d states.[18] The above characterizations reveal the existence of Ce^{3+} in both the bulk and surface of this material.

To investigate the catalytic properties of this material, the CO oxidation activity was examined for Au nanoparticles supported on meso-8CeAl and for comparison, on pure mesoporous alumina as well as pure ceria nanoparticles. TEM characterizations (Fig. S6) show that Au particles on the meso-8CeAl and meso-Al_2O_3 supports possess narrow unimodal size distributions with the same mean diameters of 7 nm, indicating similar Au dispersions on both supports. The evolution of the CO conversion as a function of temperature is presented in Figure 3a. The sample 1 wt% Au/meso-Al gives 100% CO conversion when the reaction is performed at 150 °C while 1 wt% Au/CeO_2 gives a higher activity with 100% conversion at 120 °C. Loaded with the same amount of Au nanoparticles (Table S2), our material meso-8CeAl exhibits excellent catalytic activity at room temperature with 100%

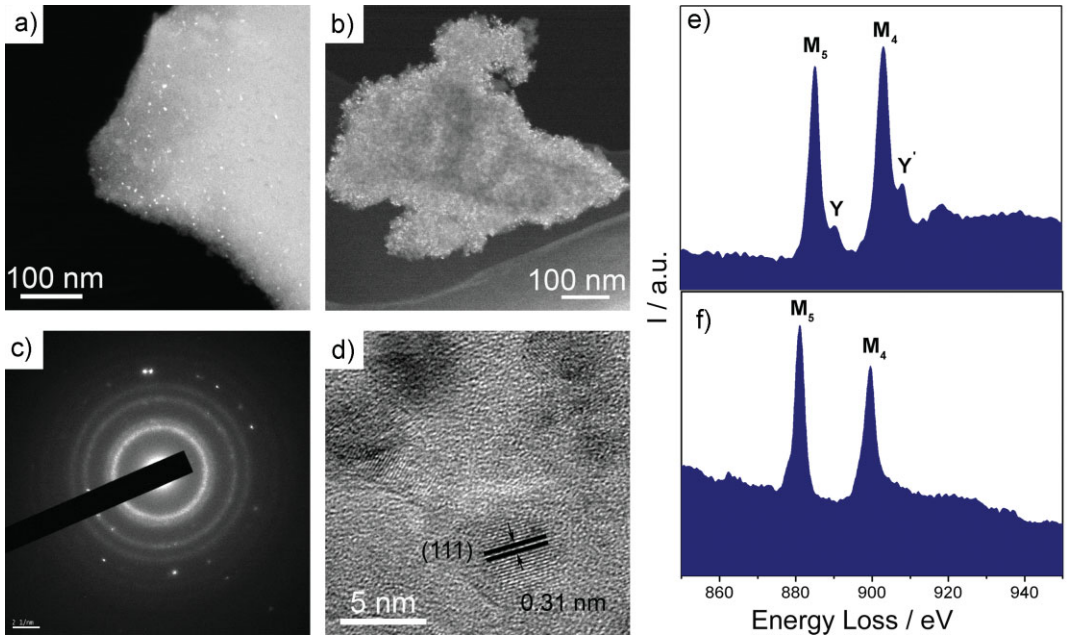

Figure 2. HAADF STEM images of a) meso-8CeAl and b) meso-16CeAl calcined at 400 °C. c) SAED and (d) HRTEM image of meso-8CeAl calcined at 400 °C. EELS of e) a CeO_2 thin film and f) meso-8CeAl calcined at 400 °C.

conversion occurring at 26 °C, which is much better than the other two catalysts. This could be attributed to the strong synergistic interaction between the noble metal Au and CeO_2. The nature of the support plays a very important role in determining the metal catalysts' activity because of the interaction between the support and the catalysts.[13a,19] In the case of the Au-supported catalyst, previous researchers have proven that this interaction effect can obviously change the state of Au,[20] which results in different catalytic properties.[4,21] High-resolution Au 4f XPS spectra (Fig. S4c) show that the sample contains a mixture of cationic and metallic gold. The curve-fit analysis indicates three components in the Au 4f spectrum, with contributions of Au^0, Au^{1+}, and Au^{3+}, respectively.[20a,22] The existence of cationic Au results in a high degree of CO adsorption and promotes the CO oxidation reactivity,[23] consistent with previous reports of enhanced catalytic activity of cationic gold.[24] Though there are only small amounts of CeO_2 nanoparticles embedded in the mesostructure, the catalytic activity is significantly enhanced. CeO_2 nanoparticles could supply reactive oxygen by releasing/taking up oxygen through a redox process involving the Ce^{4+}/Ce^{3+} couple, which can promote the oxygen adsorption and activation, and thus promotes the catalyst reactivity.[25] Besides the high catalytic activity, this novel catalyst also shows high stability. Figure 3b shows the histogram of CO conversions of Au/meso-8CeAl at 30 °C treated at different temperatures. With increasing annealing temperature, the conversion rate decreases slowly. However, this catalyst exhibits >80% conversion activity even after annealing at a high temperature of 650 °C. Recycle reactions were also performed to test the long term stability of the catalyst (Fig. S7). After five additional reaction tests, 90% CO conversion activity can still be achieved at room temperature. Therefore, we infer that the monodispersed CeO_2 nanocatalyst stabilized by ordered mesoporous alumina will be useful in the design of novel materials with enhanced catalytic activity for oxidation reactions.

In this report, we demonstrate, for the first time, that homogeneously dispersed CeO_2 nanocatalysts can be synthesized and stabilized under a high treatment temperature by the confinement effect of ordered mesoporous alumina. It is a one-step synthesis method, easier to carry out compared with grafting or impregnating methods. The homogeneous distribution of CeO_2 nanoparticles with a size of 3–5 nm is observed. Employed as catalyst support for Au in CO oxidation reaction, this novel material exhibits an excellent catalytic activity with 100% conversion at room temperature. The stability of the CeO_2 nanocatalyst within mesostructed materials fulfils the important requirements for their applications in catalysis. We envisage that this established approach is significantly expandable to the controlled synthesis and stabilization of other nanocatalysts.

Experimental

Synthesis of Meso-CeAl: Pluronic P123 (1.0 g) was dissolved in ethanol (20 mL) at room temperature (RT). Citric acid (0.84 g), $Al(NO_3)_3 \cdot 9H_2O$ (3.75 g), and quantitative $Ce(NO_3)_3 \cdot 6H_2O$ were then added with vigorous stirring. The mixture was covered with polyethylene (PE) film, stirred at RT for at least 5 h, and then placed into a 60 °C drying oven to undergo the solvent evaporation process. After two days aging, the solution turned into a light yellow solid. Calcination was carried out by slowly increasing the temperature from RT to 400 °C (1 °C min^{-1} ramping rate) and heating at 400 °C for 4 h in air. The high-temperature treatment was carried out in air for 1 h with a temperature ramp of 10 °C min^{-1}.

Synthesis of CeO_2: $(NH_4)_2Ce(NO_3)_6$ (2.74 g) and CH_3COONa (10 g) were dissolved in deionized water (70 mL) and then CH_3COOH (10 mL) was added to the solution. After stirring for 1 h at RT, the mixture was transferred to a Teflon bottle, subsequently held in a steel vessel autoclave, and then subjected to hydrothermal treatment at temperatures at 220 °C for 12 h. After the hydrothermal treatment, yellow precipitates were separated by centrifugation, washed with deionized water and ethanol several times, followed by drying at 60 °C in air overnight.

Catalyst Preparation: Au/meso-CeAl, Au/meso-Al, and Au/CeO_2 were synthesized according to literature methods [5d]. Typically, meso-CeAl

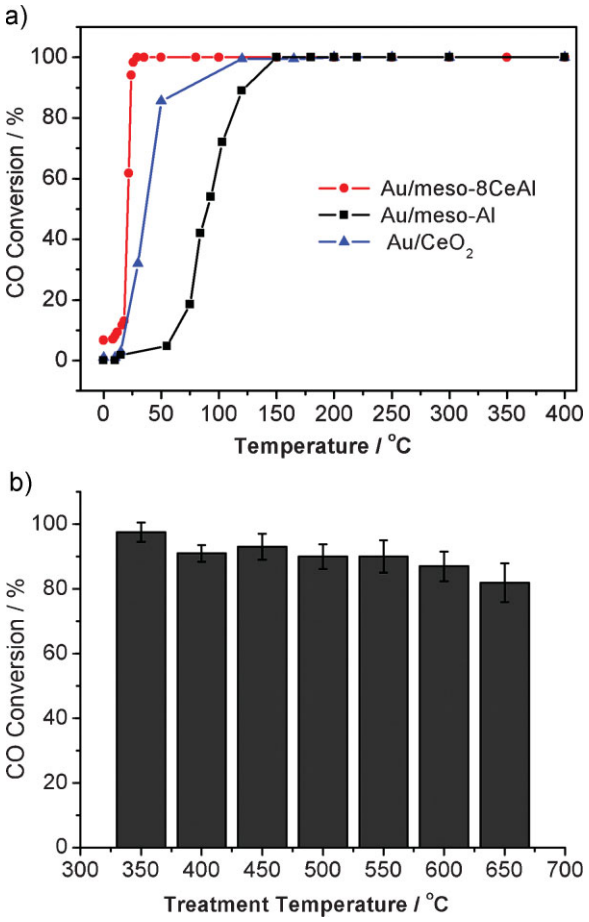

Figure 3. a) Catalytic activity of Au/meso-Al, Au/meso-8CeAl, and Au/CeO_2 for CO oxidation. b) Conversion at 30 °C after annealing at different temperatures. The error bars show the conversions in three experiments.

powder (0.3 g) was dispersed in deionized water (15 mL) while stirring and 1 M aqueous $(NH_4)_2CO_3$ solution (7.5 mL) was then added. $HAuCl_4 \cdot 3H_2O$ (2.32×10^{-3} M, 7.5 mL) was then added to the above solution dropwise. The pH value was kept at 8–9 during the whole process. The resulting precipitate was aged at RT for 1 h, and then filtered and washed three times with deionized water at 60–70 °C. The product was dried in an oven at 70–80 °C overnight and then calcined in air at 400 °C for 4 h.

Catalytic Test: A flow reactor system was built for the catalytic testing. In a typical CO oxidation experiment, Au/meso-CeAl was used as catalyst, and the experiment was carried out under the flow of the reactant gas mixture (1.0% CO, 16% O_2, balanced with N_2) with a rate of 100 mL min^{-1}. The weight of catalyst powder was 0.1 g and it filled the middle of the quartz tubular reactor. The composition of the gas was monitored on-line by gas chromatography.

Acknowledgements

Q.Y. and H.-H.D. contributed equally to this work. This work was supported by the MOST of China (2006CB601104) and the NSFC (20821091 and 20610068). Supporting Information is available online at Wiley InterScience or from the author.

Received: December 10, 2009
Published online: February 22, 2010

[1] a) Z. L. Wang, X. D. Feng, *J. Phys. Chem. B* **2003**, *107*, 13563. b) K. Kaneko, K. Inoke, B. Freitag, A. B. Hungria, P. A. Midgley, T. W. Hansen, J. Zhang, S. Ohara, T. Adschiri, *Nano Lett.* **2007**, *7*, 421. c) X. W. Liu, K. B. Zhou, L. Wang, B. Wang, Y. D. Li, *J. Am. Chem. Soc.* **2009**, *131*, 3140.
[2] a) T. Yu, J. Joo, Y. I. Park, T. Hyeon, *Angew. Chem. Int. Ed.* **2005**, *44*, 7411; *Angew. Chem.* **2005**, *117*, 7577. b) S. W. Yang, L. Gao, *J. Am. Chem. Soc.* **2006**, *128*, 9330. c) Z. Y. Huo, C. Chen, X. W. Liu, D. R. Chu, H. H. Li, Q. Peng, Y. D. Li, *Chem. Commun.* **2008**, 3741.
[3] G. C. Bond, D. T. Thompson, *Catal. Rev. Sci. Eng.* **1999**, *41*, 319.
[4] S. Carrettin, P. Concepcion, A. Corma, J. M. L. Nieto, V. F. Puntes, *Angew. Chem. Int. Ed.* **2004**, *43*, 2538; *Angew. Chem.* **2004**, *116*, 2592.
[5] a) K. B. Zhou, X. Wang, X. M. Sun, Q. Peng, Y. D. Li, *J. Catal.* **2005**, *229*, 206. b) K. B. Zhou, R. Xu, X. M. Sun, H. D. Chen, Q. Tian, D. X. Shen, Y. D. Li, *Catal. Lett.* **2005**, *101*, 169. c) R. Wang, P. A. Crozier, R. Sharma, J. B. Adams, *Nano Lett.* **2008**, *8*, 962. d) R. Si, M. Flytzani-Stephanopoulos, *Angew. Chem. Int. Ed.* **2008**, *47*, 2884; *Angew. Chem.* **2008**, *120*, 2926.
[6] U. Junges, W. Jacobs, I. Voigt-Martin, B. Drutzsch, F. Schüth, *Chem. Commun.* **1995**, 2283.
[7] J. M. Sun, D. Ma, H. Zhang, X. Liu, X. Han, X. H. Bao, G. Weinberg, N. Pfänder, D. S. Su, *J. Am. Chem. Soc.* **2006**, *128*, 15 756.
[8] K. B. Lee, S. M. Lee, J. Cheon, *Adv. Mater.* **2001**, *13*, 517.
[9] H. Song, R. M. Rioux, J. D. Hoefelmeyer, R. Komor, K. Niesz, M. Grass, P. Yang, G. A. Somorjai, *J. Am. Chem. Soc.* **2006**, *128*, 3027.
[10] A. Fukuoka, T. Higuchi, T. Ohtake, T. Oshio, J. Kimura, Y. Sakamoto, N. Shimomura, S. Inagaki, M. Ichikawa, *Chem. Mater.* **2006**, *18*, 337.
[11] N. Petkov, N. Stock, T. Bein, *J. Phys. Chem. B* **2005**, *109*, 10 737.
[12] Z. Li, C. Kübel, V. I. Pârvulescu, R. Richards, *ACS Nano* **2008**, *2*, 1205.
[13] a) P. Concepción, A. Corma, J. Silvestre-Albero, V. Franco, J. Y. Chane-Ching, *J. Am. Chem. Soc.* **2004**, *126*, 5523. b) J. Y. Chane-Ching, M. Airiau, A. Sahibed-dine, M. Daturi, E. Brendlé, F. Ozil, A. Thorel, A. Corma, *Langmuir* **2005**, *21*, 1568.
[14] H. Pérez-Pastenes, A. Ochoa-Tapia, T. Viveros, A. Montoya, *J. Sol-Gel Sci. Technol.* **2006**, *37*, 49.
[15] Q. Yuan, A. X. Yin, C. Luo, L. D. Sun, Y. W. Zhang, W. T. Duan, H. C. Liu, C. H. Yan, *J. Am. Chem. Soc.* **2008**, *130*, 3465.
[16] L. J. Wu, H. J. Wiesmann, A. R. Moodenbaugh, R. F. Klie, Y. M. Zhu, Y. M. D. O. Welch, M. Suenaga, *Phys. Rev. B* **2004**, *69*, 125 415.
[17] E. Paparazzo, G. M. Ingo, N. Zacchett, *J. Vac. Sci. Technol. A* **1991**, *9*, 1416.
[18] a) M. M. Natile, G. Boccaletti, A. Glisenti, *Chem. Mater.* **2005**, *17*, 6272. b) L. M. Qiu, F. Liu, L. Z. Zhao, Y. Ma, J. N. Yao, *Appl. Surf. Sci.* **2006**, *252*, 4931.
[19] J. B. Park, J. Graciani, J. Evans, D. Stacchiola, S. D. Senanayake, L. Barrio, P. Liu, J. F. Sanz, J. Hrbek, J. A. Rodriguez, *J. Am. Chem. Soc.* **2010**, *132*, 356.
[20] a) Q. Fu, H. Saltsburg, M. Flytzani-Stephanopoulos, *Science* **2003**, *301*, 935. b) V. Subramanian, E. E. Wolf, P. V. Kamat, *J. Am. Chem. Soc.* **2004**, *126*, 4943.
[21] M. Comotti, W. C. Li, B. Spliethoff, F. Schüth, *J. Am. Chem. Soc.* **2006**, *128*, 917.
[22] G. J. Hutchings, M. S. Hall, A. F. Carley, P. Landon, B. E. Solsona, C. J. Kiely, A. Herzing, M. Makkee, J. A. Moulijn, A. Overweg, J. C. Fierro-Gonzalez, J. G. B. C. Gates, *J. Catal.* **2006**, *242*, 71.
[23] J. Guzman, S. Carrettin, A. Corma, *J. Am. Chem. Soc.* **2005**, *127*, 3286.
[24] J. Guzman, B. C. Gates, *J. Phys. Chem. B* **2002**, *106*, 7659.
[25] a) T. X. T. Sayle, S. C. Parker, S. C. C. R. A. Catlow, *Surf. Sci.* **1994**, *316*, 329. b) J. Guzman, S. Carrettin, J. C. Fierro-Gonzalez, Y. Hao, B. C. Gates, A. Corma, *Angew. Chem. Int. Ed.* **2005**, *44*, 4778; *Angew. Chem.* **2005**, *117*, 4856.